CONDENSED MATTER PHYSICS

Unconventional scaling of the superfluid density with the critical temperature in transition metal dichalcogenides

F. O. von Rohr[1,2], J.-C. Orain[3], R. Khasanov[3], C. Witteveen[1], Z. Shermadini[3], A. Nikitin[3], J. Chang[2], A. R. Wieteska[4], A. N. Pasupathy[4], M. Z. Hasan[5], A. Amato[3], H. Luetkens[3], Y. J. Uemura[4], Z. Guguchia[3,4,5]*

We report on muon spin rotation experiments probing the magnetic penetration depth $\lambda(T)$ in the layered superconductors in 2H-$NbSe_2$ and 4H-$NbSe_2$. The current results, along with our earlier findings on 1T′-$MoTe_2$ (Guguchia *et al.*), demonstrate that the superfluid density scales linearly with T_c in the three transition metal dichalcogenide superconductors. Upon increasing pressure, we observe a substantial increase of the superfluid density in 2H-$NbSe_2$, which we find to correlate with T_c. The correlation deviates from the abovementioned linear trend. A similar deviation from the Uemura line was also observed in previous pressure studies of optimally doped cuprates. This correlation between the superfluid density and T_c is considered a hallmark feature of unconventional superconductivity. Here, we show that this correlation is an intrinsic property of the superconductivity in transition metal dichalcogenides, whereas the ratio T_c/T_F is approximately a factor of 20 lower than the ratio observed in hole-doped cuprates. We, furthermore, find that the values of the superconducting gaps are insensitive to the suppression of the charge density wave state.

INTRODUCTION

Transition metal dichalcogenides (TMDs) are a class of layered materials, which presently attract great interest because of their versatile physical, chemical, and mechanical properties (*1*–*11*). The TMDs share the MX_2 formula, with M being a transition metal (M = Ti, Zr, Hf, V, Nb, Ta, Mo, W, or Re) and X being a chalcogen (X = S, Se, or Te). These compounds crystallize in different structural phases resulting from different stacking of the individual MX_2 layers, with van der Waals bonding between them.

A variety of previously unknown physical phenomena have been reported in TMD systems. Most recently, topological physics with Dirac-type dispersion, exotic optical, and transport behavior originating from valley splitting were predicted and observed (*1*, *4*). Correlated physics has been studied intensively, especially in 2H-TaS_2, 2H-$NbSe_2$, and, more recently, 1T′-$MoTe_2$ (*5*, *12*–*15*). 2H-$NbSe_2$ is a superconductor with a critical temperature $T_c \approx 7.3$ K and hosts a two-dimensional (2D) charge density wave (CDW) with a critical temperature of $T_{CDW} \approx 33$ K (*16*–*21*). The polymorph 4H-$NbSe_2$ undergoes a CDW transition at $T_{CDW} \approx 40$ K and becomes superconducting at $T_c \approx 6$ K. The superconducting transition temperature of 2H-$NbSe_2$ is remarkably high in comparison with other TMDs, where commonly transition temperatures below 4 K are observed. Recently, it was found that both the superconducting state and the CDW ordering remain intact even for a single layer of this material (*8*). The superconducting transition temperature is thereby lowered in the 2D limit to $T_c \approx 1.1$ K. Previously, the effect of hydrostatic pressure on the CDW ordering and superconductivity was studied in 2H-$NbSe_2$ by means of magnetization and resistivity measurements (*22*, *23*). It was found that upon increasing pressures, CDW ordering is suppressed. The suppression of CDW ordering commonly causes a strong increase of the superconducting transition temperature T_c [see, e.g., (*24*–*26*)]. The generic occurrence of a "fragile" SC phase in the systems with competing SC and CDW ground states was recently reported (*27*). In 2H-$NbSe_2$, T_c increases only slightly ($\Delta T_c < 1$ K) with increasing pressure without any anomaly across the critical pressure at which the CDW state disappears. Moreover, both CDW order parameter amplitude and its static phase coherence length are unaffected when the superconductivity is suppressed in a high magnetic field (*18*). Recent x-ray experiments also suggest that different phonon branches are responsible for superconductivity and CDW orders (*23*). These findings suggested that superconductivity is only weakly affected by the suppression of the CDW ordering (*18*–*21*, *33*).

Layered superconductors with highly anisotropic electronic properties have been found to be potential hosts for unconventional superconductivity. Cuprates are the most prominent example, consisting of CuO_2 layers and the iron pnictide superconductors, with tetrahedra coordinated Fe*Pn*4 layers. Other examples for unconventional superconductivity in layered systems are a monolayer of FeSe on strontium titanate substrates (*28*) and the reported superconductivity in twisted bilayer graphene (*29*). Recently, we have reported on muon spin rotation (μSR) measurements on the TMD superconductor T_d-$MoTe_2$, which is considered to be a type II Weyl semimetal (*10*, *11*, *30*). We had found a linear scaling of superfluid density at $T = 0$ and the transition temperature T_c, similar to the relation found earlier in the cuprates (*31*) and other Fe-based superconductors (*32*–*34*).

Here, we report on the substantial increase of the superfluid density n_s/m^* in van der Waals system 2H-$NbSe_2$ (Fig. 1A) under hydrostatic pressure, which appears not to be correlated with the suppression of the CDW ordered state. We find the superfluid density in 2H-$NbSe_2$, 4H-$NbSe_2$, and 1T′-$MoTe_2$ to scale linearly with T_c,

[1]Department of Chemistry, University of Zürich, CH-8057 Zürich, Switzerland. [2]Physik-Institut der Universität Zürich, Winterthurerstrasse 190, CH-8057 Zürich, Switzerland. [3]Laboratory for Muon Spin Spectroscopy, Paul Scherrer Institute, CH-5232 Villigen PSI, Switzerland. [4]Department of Physics, Columbia University, New York, NY 10027, USA. [5]Laboratory for Topological Quantum Matter and Spectroscopy, Department of Physics, Princeton University, Princeton, NJ 08544, USA.
*Corresponding author. Email: zurab.guguchia@psi.ch

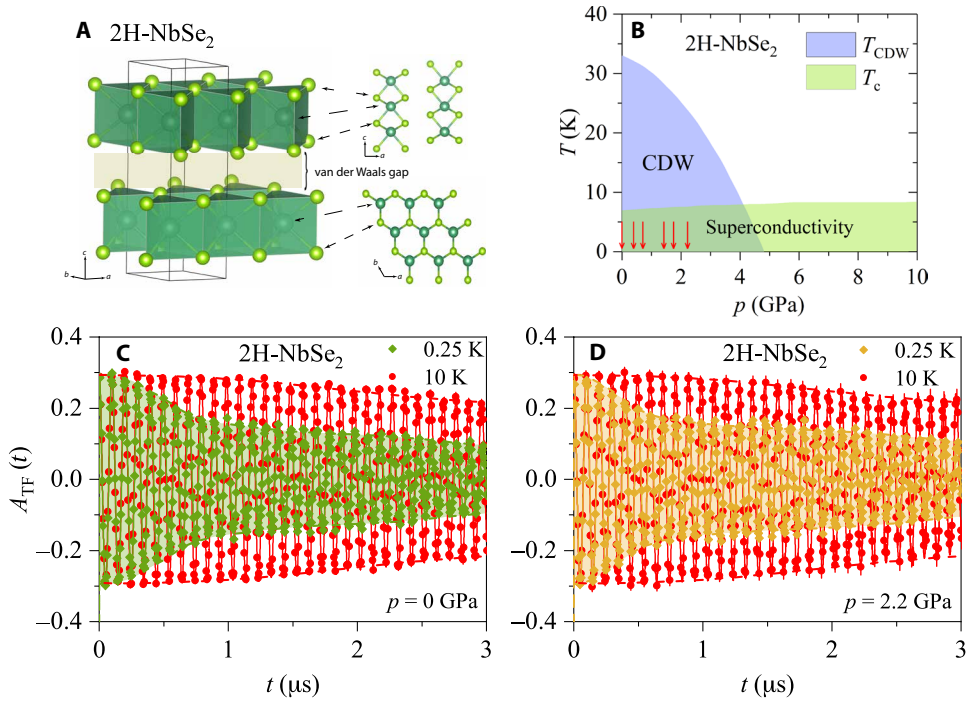

Fig. 1. Schematic phase diagram and TF μSR time spectra for $NbSe_2$. (**A**) Crystal structure of 2H-$NbSe_2$. (**B**) Pressure dependence of T_c and the CDW temperature T_{CDW} (*5*). The red arrows mark the pressures at which the *T* dependence of the penetration depth was measured. The TF spectra, above and below T_c at pressures of (**C**) $p = 0$ GPa and (**D**) $p = 2.2$ GPa, are shown. The solid lines in (C) and (D) represent fits to the data by means of Eq. 4. The dashed lines are guides to the eyes.

which indicates that this linear relation has general validity for TMD superconductors. Such relations are considered to be a hallmark feature of unconventional superconductivity (*31*, *35*, *36*) in cuprate and iron-pnictide superconductors. Upon application of pressure on 2H-$NbSe_2$, the n_s/m^* versus T_c dependence shows the deviation from the abovementioned linear behavior. We find this linear deviation to be very similar to the deviation observed for optimally doped cuprates. Our findings, therefore, pose a challenge for understanding the underlying quantum physics in these layered TMDs and might lead to a better understanding of generic aspects of non–Bardeen-Cooper-Schrieffer (BCS) behaviors in unconventional superconductors.

RESULTS AND DISCUSSION

In Fig. 1B, we show the schematic phase diagram of the pressure dependence of the CDW transition temperature T_{CDW} and the superconducting transition temperature T_c for $NbSe_2$, according to Qi *et al.* (*5*). The red arrows mark the pressures at which the *T* dependence of the penetration depth and the superfluid density was measured. As it can be seen, the CDW transition is strongly reduced within the investigated pressure range between $p = 0$ and 2.2 GPa. In Fig. 1 (C and D), two representatives of the transverse-field (TF) μSR time spectra for 2H-$NbSe_2$ at ambient pressure and at the maximum applied pressure of $p = 2.2$ GPa are shown. Both measurements were performed in the pressure cell. For both pressures, the TF muon time spectra in a field of $\mu_0 H = 70$ mT are shown above ($T = 10$ K) and below ($T = 0.25$ K) the superconducting transition temperature T_c. Above T_c, the oscillations show a small relaxation due to the random local fields from the nuclear magnetic moments. Below T_c, the relaxation rate strongly increases with decreasing temperature due to the presence of a nonuniform local magnetic field distribution as a result of the formation of a flux-line lattice (FLL) in the Shubnikov phase.

From the obtained TF muon time spectra, we have derived the temperature dependence of the muon spin depolarization rate σ_{sc}, which is proportional to the second moment of the field distribution (see Methods). In Fig. 2, we show the temperature dependence of the muon spin depolarization rate σ_{sc} of 4H-$NbSe_2$ at ambient pressure and 2H-$NbSe_2$ at pressures of $p = 0$, 0.4, 0.7, 1.4, and 2.2 GPa. Below T_c, the relaxation rate σ_{sc} starts to increase from zero with decreasing temperature owing to the formation of the FLL. The critical temperatures for 2H-$NbSe_2$ and 4H-$NbSe_2$ are $T_c \sim 6$ K and 7 K, respectively. We find that the low-temperature value of σ_{sc} between 2H-$NbSe_2$ and 4H-$NbSe_2$ increases as much as T_c. Upon application of pressure on 2H-$NbSe_2$, the superconducting transition temperature T_c increases, which is in good agreement with earlier reports (*22*, *23*). Furthermore, we observed a substantial increase of the low-temperature value of the muon spin depolarization rate σ_{sc} with increasing pressure. This can be seen most clearly at base temperature, where the muon spin depolarization rate $\sigma_{sc}(T = 0.25\ \text{K})$ increases by ~30% from $p = 0$ GPa to $p = 2.2$ GPa. At all pressures, the form of the temperature dependence of σ_{sc}, which reflects the topology of the SC gap, shows the saturation at low temperatures, indicating the presence of the isotropic pairing in $NbSe_2$ at all applied pressure.

The second moment of the resulting inhomogeneous field distribution is related to the magnetic penetration depth λ as $\langle \Delta B^2 \rangle \propto \sigma_{sc}^2 \propto \lambda^{-4}$, whereas σ_{sc} is the Gaussian relaxation rate due to the formation of FLL (*37*). To investigate the symmetry of the superconducting

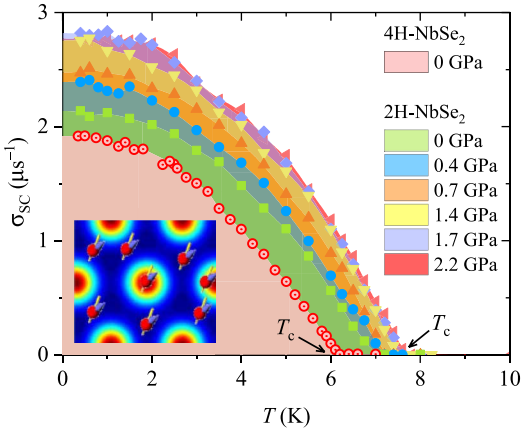

Fig. 2. Superconducting muon spin depolarization rate σ_{SC} for $NbSe_2$. Temperature dependence of $\sigma_{SC}(T)$ measured in 4H-$NbSe_2$ at ambient pressure and in 2H-$NbSe_2$ at various hydrostatic pressures in an applied magnetic field of $\mu_0 H = 70$ mT.

gap, we have therefore derived the temperature-dependent London magnetic penetration depth $\lambda(T)$, which is related to the relaxation rate by

$$\frac{\sigma_{sc}(T)}{\gamma_\mu} = 0.06091\frac{\Phi_0}{\lambda^2(T)} \quad (1)$$

Here, γ_μ is the gyromagnetic ratio of the muon, and Φ_0 is the magnetic-flux quantum. Thus, the flat T dependence of σ_{sc} observed at various pressures for low temperatures (see Fig. 2) is consistent with a nodeless superconductor, in which $\lambda^{-2}(T)$ reaches its zero-temperature value exponentially.

To proceed with a quantitative analysis, we consider the local (London) approximation ($\lambda \gg \xi$, where ξ is the coherence length) and use the empirical α model. The model, widely used in previous investigations of the penetration depth of multiband superconductors (*38*–*42*), assumes that the gaps occurring in different bands, besides a common T_c, are independent of each other. The superfluid density is calculated for each component separately (*38*) and added together with a weighting factor. For our purposes, a two-band model suffices, yielding

$$\frac{\lambda^{-2}(T)}{\lambda^{-2}(0)} = \omega_1\frac{\lambda^{-2}(T,\Delta_{0,1})}{\lambda^{-2}(0,\Delta_{0,1})} + \omega_2\frac{\lambda^{-2}(T,\Delta_{0,2})}{\lambda^{-2}(0,\Delta_{0,2})} \quad (2)$$

Here, $\lambda(0)$ is the London magnetic penetration depth at zero temperature, $\Delta_{0,i}$ is the value of the ith SC gap (i = 1, 2) at T = 0 K, and ω_i is the weighting factor, which measures their relative contributions to λ^{-2} (i.e., $\omega_1 + \omega_2 = 1$).

The results of this analysis are presented in Fig. 3A, where the temperature dependence of λ^{-2} is plotted for 4H-$NbSe_2$ at ambient pressure and for 2H-$NbSe_2$ at pressures of p = 0, 0.4, 0.7, 1.4, and 2.2 GPa. The dashed and the solid lines for ambient pressure results represent fits for the temperature-dependent London magnetic penetration at ambient pressure using an s-wave and an s + s-wave model, respectively (*30*). As it can be seen, the s + s-wave provides a much better description of the data, thereby ruling out the simple s-wave model as an adequate description of $\lambda^{-2}(T)$ for 2H-$NbSe_2$. The two-gap s + s-wave scenario with a small gap $\Delta_1 \simeq 0.55(3)$ meV and a large gap $\Delta_2 \simeq 1.25(5)$ meV for p = 0 GPa [with the pressure-independent weighting factor of $\omega_2 = 0.8(1)$] describes the experimental data remarkably well.

The presence of two isotropic gaps in 2H-$NbSe_2$ and their values are in very good agreement with previous results (*43*–*47*). According to angle-resolved photoemission spectroscopy (ARPES) data, several independent electronic bands (four Nb-derived bands with roughly cylindrical Fermi surfaces centered at the Γ and K points and one Se-derived band with a small ellipsoid pocket around the Γ point) cross the Fermi surface in 2H-$NbSe_2$, and two-gap superconductivity can be understood by assuming that the SC gaps open at two distinct types of bands. We find that two-gap s + s-wave superconductivity is preserved up to the highest applied pressure of p = 2.2 GPa. All the s + s-wave fits for all pressures are shown in Fig. 3C. Furthermore, the pressure dependence of all the parameters extracted from the data analysis within the α model is plotted in Fig. 3 (B and C). The critical temperature T_c increases with pressure only by ~0.7 K at the maximum applied pressure of p = 2.2 GPa, as shown in Fig. 3B. We, however, observe a substantial increase of the superfluid density λ^{-2} with increasing pressures, as shown in Fig. 3B. At the maximum applied pressure of p = 2.2 GPa, the increase of λ^{-2} is $\Delta p \approx 31.4(8)\%$ compared to the value at ambient pressure. The absolute size of the small gap $\Delta_1 \simeq 0.5(3)$ meV and that of the large gap $\Delta_2 \simeq 1.25(5)$ meV remain nearly unchanged by pressure, as shown in Fig. 3C. The two-gap s + s-wave scenario also describes the data for 4H-$NbSe_2$, which was not reported previously. The gap values for 4H-$NbSe_2$ are $\Delta_1 \simeq 0.19(3)$ and $\Delta_2 \simeq 0.89(1)$ meV.

The London magnetic penetration depth λ is given as a function of n_s, m^*, ξ, and the mean free path l, according to

$$\frac{1}{\lambda^2} = \frac{4\pi n_s e^2}{m^* c^2} \times \frac{1}{1+\xi/l} \quad (3)$$

For systems close to the clean limit, $\xi/l \to 0$, the second term essentially becomes unity, and the simple relation $1/\lambda^2 \propto n_s/m^*$ holds. Considering the upper critical fields H_{c2} of 2H-$NbSe_2$, as reported in detail by Soto *et al.* (*48*), we can estimate the in-plane coherence length to be $\xi_{ab} \simeq 7.9$ nm at ambient pressure p = 0 GPa. At ambient pressure, the in-plane mean free path l was estimated to be $l_{ab} \simeq$ 183 nm (*48*). No estimates are currently available for l under pressure. However, the in-plane l is most probably independent of pressure, considering the fact that the effect of compression is mostly interlayered; i.e., the intralayer Nb-Se bond length remains nearly unchanged (especially in the here investigated pressure region) (*22*). This very small effect of compression can be attributed to the unique anisotropy resulting from the stacking of layers with van der Waals type interactions between them. Thus, in view of the short coherence length and relatively large l, we can reliably assume that 2H-$NbSe_2$ lies close to the clean limit (*30*, *49*). With this assumption, we obtain the ground-state value $n_s/(m^*/m_e) \simeq 5.7 \times 10^{27}$ m^{-3} and 7.5×10^{27} m^{-3} for p = 0 and 2.2 GPa, respectively.

The strong enhancement of the superfluid density $\lambda^{-2}(0) \propto n_s/(m^*/m_e)$ in 2H-$NbSe_2$ under pressure, as discussed above, is an essential finding of this paper. Note that the impairment of the CDW ordering and the associated lowering of the CDW ordering transition T_{CDW} under pressure may cause the restoring of some electronic density of states at the Fermi surface. However, the electron and hole states that condense into the CDW ordered state comprise only ≈1% of the total density of states at the Fermi surface in 2H-$NbSe_2$

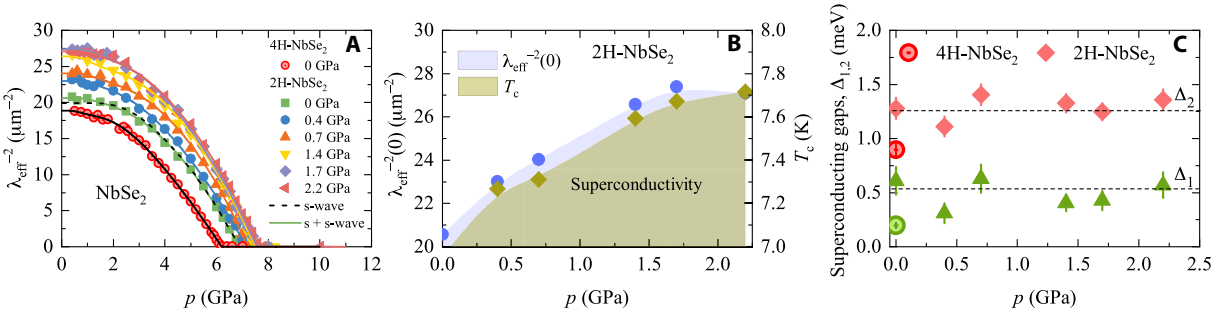

Fig. 3. Pressure evolution of various quantities. (**A**) The temperature dependence of λ^{-2} measured at ambient pressure for 4H-$NbSe_2$ and at various applied hydrostatic pressures for 2H-$NbSe_2$. The solid lines correspond to a two-gap (s + s)-wave model, and the dashed line represents a fit using a single-gap s-wave model. (**B**) Pressure dependence of T_c and the zero-temperature value of $\lambda^{-2}(0)$. (**C**) Pressure dependence of the zero-temperature values of the small superconducting gap Δ_1 and the large superconducting gap Δ_2.

(*50*–*52*). The expected maximal increase of the total density of states caused by a complete suppression of the CDW would be $\Delta D(E_F) \approx 1\%$, which cannot solely attribute for the observed ~30% enhancement of the superfluid density in 2H-$NbSe_2$. Thus, the large pressure effect on $n_s/(m^*/m_e)$ has a more complex origin. We also observed that both superconducting gaps Δ_1 and Δ_2 are nearly pressure independent up to a pressure of $p = 2.2$ GPa (Fig. 3C), while the CDW transition temperature is largely reduced in the pressure range $p = 0$ to 2.2 GPa (*22*, *23*). This implies that the gap values are insensitive to the suppression of the CDW state. This observation strongly supports the idea that superconducting and CDW orders are somewhat isolated from each other and that the CDW pairing has only a minimal effect on the superconductivity in 2H-$NbSe_2$ (*23*). Furthermore, we find the superfluid density in three TMD superconductors—2H-$NbSe_2$, 4H-$NbSe_2$, and 1T′-$MoTe_2$—to scale linearly with T_c, as shown in Fig. 4 (A and B), which is not expected within BCS theory. This means that the ratio between the superfluid density and the critical temperature T_c in 2H-$NbSe_2$ and 4H-$NbSe_2$ is nearly the same as that for the TMD superconductor 1T′-$MoTe_2$ (*30*), indicating a common mechanism and related electronic origin for the superconductivity. We observed that upon application of pressure on 2H-$NbSe_2$, the dependence between n_s/m^* and T_c deviates from the linear correlation, as shown in Fig. 4B. Note that such a deviation was previously found in optimally doped cuprate and Fe-based superconductors under pressure. As an example, the inset of Fig. 4B demonstrates the deviation from the Uemura line in the optimally doped $La_{2-x}Ba_xCuO_4$ ($x = 0.155$) under pressure (*73*). Note that in the case of 1T′-$MoTe_2$, the linear relation with the right slope holds even under pressure, up to the highest investigated pressure of 1.3 GPa, but within this pressure range, the maximum T_c of 1T′-$MoTe_2$ is 2.7 K, which is far below from the optimal superconducting region, where T_c is about 8 K. In the case of 2H-$NbSe_2$, the system has a $T_c = 7$ K already at ambient pressure, which is still below but quite close to the optimal superconducting region of the phase diagram. Application of pressure pushes the system toward the optimal superconductivity, and as can be seen from our data, the pressure of 1.7 GPa is enough to reach the maximum $T_c \sim 8$ K in 2H-$NbSe_2$. Since, historically, the linear increase of T_c with $n_s/(m^*/m_e)$ is observed only in the underdoped region of the phase diagram of unconventional superconductors, the deviation from the linear relationship for 2H-$NbSe_2$ under pressure can be explained by locating the system 2H-$NbSe_2$ within or close to the optimal superconducting region under pressure. The fact that TMDs studied in this work exhibit markedly similar features in the relation between the superfluid density and the critical temperature to those reported in other unconventional superconductors implies that TMDs exhibit unconventional superconducting properties. We also show in 2H-$NbSe_2$ that the extracted gap sizes do not depend on T_c, which is an additional evidence of unconventional behavior.

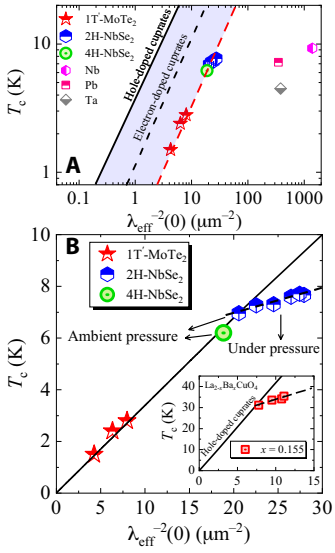

Fig. 4. Superfluid density versus T_c. (**A**) Logarithmic plot of T_c against the $\lambda^{-2}(0)$ obtained from our μSR experiments in 2H-$NbSe_2$, 4H-$NbSe_2$, and $MoTe_2$. The dashed red line represents the linear fit to the $MoTe_2$ data. Uemura relation for hole- and electron-doped cuprates are shown as solid (*31*, *53*–*55*) and dashed lines (*57*), respectively. The points for various conventional BCS superconductors are also shown. (**B**) Linear plot of T_c against the $\lambda^{-2}(0)$. Inset shows the T_c against the $\lambda^{-2}(0)$ as a function of pressure for optimally doped cuprate superconductor $La_{2-x}Ba_xCuO_4$ (*73*).

The nearly linear relationship between T_c and the superfluid density was originally observed in hole-doped cuprates (*31*, *35*), where the ratio between T_c and their effective Fermi temperature T_F is about $T_c/T_F \sim 0.05$, which means about four to five times reduction of T_c from the ideal Bose condensation temperature for a noninteracting Bose gas. These results were discussed in terms of the crossover from Bose-Einstein condensation (BEC) to BCS-like condensation (*53*–*55*). Within the picture of BEC to BCS crossover, systems exhibiting small T_c/T_F (large T_F) are considered to be in the BCS-like side, while the linear relationship between T_c and T_F is

expected only in the BEC-like side. This relationship has been used in the past for the characterization of BCS-like, so-called conventional superconductors and BEC-like, so-called unconventional superconductors. The present results on 2H-$NbSe_2$ and 4H-$NbSe_2$, together with our previously reported results on 1T′-$MoTe_2$, demonstrate that a linear relation between T_c and the superfluid density holds for these TMD systems. However, we find the ratio T_c/T_F to be reduced further by a factor of ~20. These systems fall into the clean limit, and therefore, the linear relation is unrelated to pair breaking and can be regarded to hold between T_c and n_s/m^*. This implies that the BEC-like linear relationship may exist in systems with T_c/T_F reduced even by a factor of 20 from the ratio in hole-doped cuprates.

In (*54*–*56*), one of the present authors pointed out that there seem to exist at least two factors that determine T_c in unconventional superconductors: One is the superfluid density, and the other is the closeness to the competing state. The second factor can be seen in the energy of the magnetic resonance mode, which represents the difference in free energy between the superconducting state and the competing magnetically ordered state. In the case of hole-doped cuprates, the competing state is characterized by antiferromagnetic order but frustrated by the introduction of doped holes. In the case of electron-doped cuprates, the competing state develops in an antiferromagnetic network diluted by the doped carriers. In the case of present TMD systems, the competing state comes from CDW or structural orders. These systematic differences of competing states might be related to the three different ratios of T_c/T_F seen in the three different families of superconductors shown in Fig. 4.

Note that the similar relation between the superfluid density and the critical temperature, observed in layered dichalcogenides and the cuprates, extends a long list of analogies between this different class of materials: pressure and doping phase diagrams (*58*), Nernst effect (*59*), optics (*60*), Hall effect (*61*), "kinks" in dispersion (*62*), pseudogap, and Fermi surface "arcs" (*63*–*65*). Moreover, the presence of two s-wave superconducting gaps in TMDs, observed by μSR, STM, and ARPES, is analogous to the two-gap (s + s-wave) superconducting gap symmetry of the unconventional Fe-based superconductors (*32*–*34*). Thus, this report contributes to an extensive list of analogies between known unconventional superconductors (*58*–*67*) (i.e., the cuprates and the pnictides) and layered TMDs. Our findings are all the more the clearest, systematic observation of unconventional superconducting properties in these compounds to date.

In summary, we provide the first microscopic investigation of the superconductivity under hydrostatic pressure in the layered superconductors 2H-$NbSe_2$ and 4H-$NbSe_2$. Specifically, the zero-temperature magnetic penetration depth $\lambda_{eff}(0)$ and the temperature dependence of λ_{eff}^{-2} were studied by means of μSR experiments in 2H-$NbSe_2$ as a function of pressure up to $p \simeq 2.2$ GPa and in 4H-$NbSe_2$ at ambient pressure. The superfluid densities in both samples and at all pressures are best described by a two-gap s + s-wave scenario. Considering the current data on 2H-$NbSe_2$ and 4H-$NbSe_2$ at ambient pressure and our previous observations on 1T′-$MoTe_2$ (*30*) at ambient as well as at low pressures, we conclude that the superfluid density $n_s/m^* \propto 1/\lambda^2$ scales linearly with T_c in the three TMD superconductors 1T′-MoTe2, 2H-$NbSe_2$, and 4H-$NbSe_2$. We also find that the application of pressure on 2H-$NbSe_2$ causes a substantial increase of the superfluid density n_s/m^*, which correlates with T_c. However, the n_s/m^* versus T_c dependence shows a linear deviation from the Uemura relation. Such a deviation was also previously found in optimally doped cuprate and Fe-based superconductors under pressure. We explain this deviation by considering the fact that the system 1T′-$MoTe_2$ at low pressures and 4H-$NbSe_2$ and 2H-$NbSe_2$ at ambient pressure are located below the optimal SC region of the phase diagram and thus show excellent linear scaling between n_s/m^* and T_c, while 2H-$NbSe_2$ is pushed into the optimal SC region by pressure, causing the deviation from the Uemura relation between n_s/m^* and T_c; the same is observed for cuprates. Our results demonstrate that a linear relation holds for the above-studied TMD superconductors located below the optimal superconducting region of the phase diagram. A ratio T_c/T_F for TMDs is reduced by a factor of 20 from the ratio in hole-doped cuprates. This implies that the superfluid density of TMDs is about an order of magnitude higher than that in the cuprates with respect to their critical temperatures T_c. The fact that TMDs exhibit markedly similar features in the relation between the superfluid density and the critical temperature to those reported in other unconventional superconductor implies that TMDs exhibit rather unconventional superconducting properties. We also find that the values of the superconducting gaps are insensitive to the suppression of the CDW ordered state, indicating that CDW pairing has only a minimal effect on the superconductivity in 2H-$NbSe_2$. These results hint toward a common mechanism and electronic origin for superconductivity in TMDs, which might have far-reaching consequences for the future development of devices based on these materials.

METHODS

Sample preparation

Single-phase polycrystalline samples of 2H-$NbSe_2$ and 4H-$NbSe_2$ were prepared by means of high-temperature solid-state synthesis. Stoichiometric amounts of niobium powder (99.99%) and selenium shots (99.999%) were mixed (for 4H-$NbSe_2$, an excess of selenium was used) and heated in a sealed quartz tube under an inert atmosphere at 750°C (2H-$NbSe_2$) and at 900°C (4H-$NbSe_2$) for 3 days.

Pressure cell

Pressures up to 2.2 GPa were generated in a double-wall piston cylinder type of cell made of CuBe material, especially designed to perform μSR experiments under pressure (*68*–*71*). As a pressure-transmitting medium, Daphne oil was used. The pressure was measured by tracking the SC transition of a very small indium plate by AC susceptibility. The filling factor of the pressure cell was maximized. The fraction of the muons stopping in the sample was approximately 40%.

μSR experiment

In a μSR experiment (*72*), nearly 100% spin-polarized muons μ^+ were implanted into the sample one at a time. The positively charged μ^+ thermalize at interstitial lattice sites, where they act as magnetic microprobes. In a magnetic material, the muon spin precesses in the local field B_μ at the muon site with the Larmor frequency $\nu_\mu = \gamma_\mu/(2\pi)B_\mu$ [muon gyromagnetic ratio $\gamma_\mu/(2\pi) = 135.5$ MHz T^{-1}]. Using the μSR technique, important length scales of superconductors can be measured, namely, the magnetic penetration depth λ and the coherence length ξ. If a type II superconductor is cooled below T_c in an applied magnetic field ranged between the lower (H_{c1}) and the upper (H_{c2}) critical fields, a vortex lattice is formed, which, in general, is incommensurate with the crystal lattice with vortex cores separated by much larger distances than those of the unit cell. Because the implanted muons stop at given crystallographic sites, they will

randomly probe the field distribution of the vortex lattice. These measurements need to be performed in a field applied perpendicular to the initial muon spin polarization (so-called TF configuration).

μSR experiments under pressure were performed at the μE1 beamline of the Paul Scherrer Institute (Villigen, Switzerland), where an intense high-energy (p_μ = 100 MeV/c) beam of muons was implanted in the sample through the pressure cell. The low-background Dolly instrument was used to study the polycrystalline samples of 2H-$NbSe_2$ and 4H-$NbSe_2$ at ambient pressure.

Analysis of TF-μSR data

The TF μSR data were analyzed by using the following functional form (*39*)

$$P(t) = A_s \exp\left[-\frac{(\sigma_{sc}^2 + \sigma_{nm}^2)\,t^2}{2}\right]\cos(\gamma_\mu B_{int,s}\,t + \varphi) + A_{pc}\exp\left[-\frac{\sigma_{pc}^2 t^2}{2}\right]\cos(\gamma_\mu B_{int,pc}\,t + \varphi) \quad (4)$$

Here, A_s and A_{pc} denote the initial assymmetries of the sample and the pressure cell, respectively. $\gamma/(2\pi) \simeq 135.5$ MHz/T is the muon gyromagnetic ratio, φ is the initial phase of the muon-spin ensemble, and B_{int} represents the internal magnetic field at the muon site. The relaxation rates σ_{sc} and σ_{nm} characterize the damping due to the formation of the FLL in the SC state and of the nuclear magnetic dipolar contribution, respectively. In the analysis, σ_{nm} was assumed to be constant over the entire temperature range and was fixed to the value obtained above T_c, where only nuclear magnetic moments contribute to the muon depolarization rate σ. The Gaussian relaxation rate, σ_{pc}, reflects the depolarization owing to the nuclear moments of the pressure cell. The width of the pressure cell signal increases below T_c. As shown previously (*70*), this is due to the influence of the diamagnetic moment of the SC sample on the pressure cell, leading to the temperature-dependent σ_{pc} below T_c. To consider this influence, we assumed the linear coupling between σ_{pc} and the field shift of the internal magnetic field in the SC state, $\sigma_{pc}(T) = \sigma_{pc}(T > T_c) + C(T)(\mu_0 H_{int,\,NS} - \mu_0 H_{int,\,SC})$, where $a_{pc}(T > T_c) = 0.25\ \mu s^{-1}$ is the temperature-independent Gaussian relaxation rate. $\mu_0 H_{int,\,NS}$ and $\mu_0 H_{int,\,SC}$ are the internal magnetic fields measured in the normal and in the SC state, respectively. As indicated by the solid lines in Fig. 1 (C and D), the μSR data were well described by Eq. 4. The good agreement between the fits and the data demonstrates that the model used describes the data rather well.

Analysis of λ(*T*)

λ(*T*) was calculated within the local (London) approximation ($\lambda \gg \xi$) by the following expression (*39*, *40*)

$$\frac{\lambda^{-2}(T,\Delta_{0,i})}{\lambda^{-2}(0,\Delta_{0,i})} = 1 + \frac{1}{\pi}\int_0^{2\pi}\int_{\Delta(T,\varphi)}^{\infty}\left(\frac{\partial f}{\partial E}\right)\frac{E\,dE\,d\varphi}{\sqrt{E^2 - \Delta_i(T,\varphi)^2}} \quad (5)$$

where $f = [1 + \exp(E/k_BT)]^{-1}$ is the Fermi function, φ is the angle along the Fermi surface, and $\Delta_i(T, \varphi) = \Delta_{0,i}\Gamma(T/T_c)g(\varphi)$ ($\Delta_{0,i}$ is the maximum gap value at $T = 0$). The temperature dependence of the gap was approximated by the expression $\Gamma(T/T_c) = \tanh\{1.82[1.018(T_c/T - 1)]^{0.51}\}$ (*41*), while $g(\varphi)$ describes the angular dependence of the gap and it is replaced by 1 for both an s-wave and an s + s-wave gap and $|\cos(2\varphi)|$ for a d-wave gap.

REFERENCES AND NOTES

1. A. A. Soluyanov, D. Gresch, Z. Wang, Q. Wu, M. Troyer, X. Dai, B. A. Bernevig, Type-II Weyl semimetals. *Nature* **527**, 495–498 (2015).
2. L. Huang, T. M. McCormick, M. Ochi, Z. Zhao, M.-T. Suzuki, R. Arita, Y. Wu, D. Mou, H. Cao, J. Yan, N. Trivedi, A. Kaminski, Spectroscopic evidence for a type II Weyl semimetallic state in $MoTe_2$. *Nat. Mater.* **15**, 1155–1160 (2016).
3. X. Xu, W. Yao, D. Xiao, T. F. Heinz, Spin and pseudospins in layered transition metal dichalcogenides. *Nat. Phys.* **10**, 343–350 (2014).
4. M. N. Ali, J. Xiong, S. Flynn, J. Tao, Q. D. Gibson, L. M. Schoop, T. Liang, N. Haldolaarachchige, M. Hirschberger, N. P. Ong, R. J. Cava, Large, non-saturating magnetoresistance in WTe_2. *Nature* **514**, 205–208 (2014).
5. Y. Qi, P. G. Naumov, M. N. Ali, C. R. Rajamathi, W. Schnelle, O. Barkalov, M. Hanfland, S. C. Wu, C. Shekhar, Y. Sun, V. Süß, M. Schmidt, U. Schwarz, E. Pippel, P. Werner, R. Hillebrand, T. Förster, E. Kampert, S. Parkin, R. J. Cava, C. Felser, B. Yan, S. A. Medvedev, Superconductivity in Weyl semimetal candidate $MoTe_2$. *Nat. Comm.* **7**, 11038 (2016).
6. X. Qian, J. Liu, L. Fu, J. Li, Quantum spin Hall effect in two-dimensional transition metal dichalcogenides. *Science* **346**, 1344–1347 (2014).
7. Y. J. Zhang, T. Oka, R. Suzuki, J. T. Ye, Y. Iwasa, Electrically switchable chiral light-emitting transistor. *Science* **344**, 725–728 (2014).
8. M. M. Ugeda, A. J. Bradley, Y. Zhang, S. Onishi, Y. Chen, W. Ruan, C. Ojeda-Aristizabal, H. Ryu, M. T. Edmonds, H.-Z. Tsai, A. Riss, S.-K. Mo, D. Lee, A. Zettl, Z. Hussain, Z.-X. Shen, M. F. Crommie, Characterization of collective ground states in single-layer NbSe2. *Nat. Phys.* **12**, 92–97 (2016).
9. R. Yu, S. Banerjee, H. C. Lei, R. Sinclair, M. Abeykoon, H. D. Zhou, C. Petrovic, Z. Guguchia, E. S. Bozin, Absence of local fluctuating dimers in superconducting $Ir_{1-x}(Pt,Rh)_xTe_2$. *Phys. Rev. B* **97**, 174515 (2018).
10. Y. Sun, S.-C. Wu, M. N. Ali, C. Felser, B. Yan, Prediction of Weyl semimetal in orthorhombic $MoTe_2$. *Phys. Rev. B* **92**, 161107 (2015).
11. I. Belopolski, D. S. Sanchez, Y. Ishida, X. Pan, P. Yu, S.-Y. Xu, G. Chang, T.-R. Chang, H. Zheng, N. Alidoust, G. Bian, M. Neupane, S.-M. Huang, C.-C. Lee, Y. Song, H. Bu, G. Wang, S. Li, G. Eda, H.-T. Jeng, T. Kondo, H. Lin, Z. Liu, F. Song, S. Shin, M. Zahid Hasan, Discovery of a new type of topological Weyl fermion semimetal state in $Mo_xW_{1-x}Te_2$. *Nat. Commun.* **7**, 13643 (2016).
12. B. Sipos, A. F. Kusmartseva, A. Akrap, H. Berger, L. Forró, E. Tutiš, From Mott state to superconductivity in 1T-TaS_2. *Nat. Mat.* **7**, 960–965 (2008).
13. K. Cho, M. Kończykowski, S. Teknowijoyo, M. A. Tanatar, J. Guss, P. B. Gartin, J. M. Wilde, A. Kreyssig, R. J. McQueeney, A. I. Goldman, V. Mishra, P. J. Hirschfeld, R. Prozorov, Using controlled disorder to probe the interplay between charge order and superconductivity in $NbSe_2$. *Nat. Comm.* **9**, 2796 (2018).
14. C. D. Malliakas, M. G. Kanatzidis, Nb–Nb interactions define the charge density wave structure of 2H-NbSe2. *J. Am. Chem. Soc.* **135**, 1719–1722 (2013).
15. H. Luo, J. Strychalska-Nowak, J. Li, J. Tao, T. Klimczuk, R. J. Cava, S-shaped suppression of the superconducting transition temperature in Cu-intercalated $NbSe_2$. *Chem. Mater.* **29**, 3704–3712 (2017).
16. R. C. Morris, R. V. Coleman, R. Bhandari, Superconductivity and magnetoresistance in $NbSe_2$. *Phys. Rev. B* **5**, 895–901 (1972).
17. D. E. Moncton, J. D. Axe, F. J. DiSalvo, Neutron scattering study of the charge-density wave transitions in 2H–$TaSe_2$ and 2H–$NbSe_2$. *Phys. Rev. B* **16**, 801–819 (1977).
18. C.-H. Du, W. J. Lin, Y. Su, B. K. Tanner, P. D. Hatton, D. Casa, B. Keimer, J. P. Hill, C. S. Oglesby, H. Hohl, X-ray scattering studies of 2H-$NbSe_2$, a superconductor and charge density wave material, under high external magnetic fields. *J. Phys. Condens. Matter* **12**, 5361–5370 (2000).
19. C. Berthier, P. Molinié, D. Jérome, Evidence for a connection between charge density waves and the pressure enhancement of superconductivity in 2H-$NbSe_2$. *Solid State Commun.* **18**, 1393–1395 (1976).
20. P. B. Littlewood, C. M. Varma, Gauge-invariant theory of the dynamical interaction of charge density waves and superconductivity. *Phys. Rev. Lett.* **47**, 811–814 (1981).
21. P. B. Littlewood, C. M. Varma, Amplitude collective modes in superconductors and their coupling to charge-density waves. *Phys. Rev. B* **26**, 4883–4893 (1982).
22. Y. Feng, J. Wang, R. Jaramillo, J. van Wezel, S. Haravifard, G. Srajer, Y. Liu, Z.-A. Xu, P. B. Littlewood, T. F. Rosenbaum, Order parameter fluctuations at a buried quantum critical point. *Proc. Natl. Acad. Sci. U.S.A.* **109**, 7224–7229 (2012).
23. M. Leroux, I. Errea, M. Le Tacon, S.-M. Souliou, G. Garbarino, L. Cario, A. Bosak, F. Mauri, M. Calandra, P. Rodière, Strong anharmonicity induces quantum melting of charge density wave in 2H–$NbSe_2$ under pressure. *Phys. Rev. B* **92**, 140303 (2015).
24. F. von Rohr, R. Nesper, A. Schilling, Strong anharmonicity induces quantum melting of charge density wave in 2H–$NbSe_2$ under pressure. *Phys. Rev. B* **89**, 094505 (2014).
25. F. von Rohr, A. Schilling, R. Nesper, C. Baines, M. Bendele, Superconductivity in rubidium-substituted $Ba_{1-x}Rb_xTi_2Sb_2O$. *Phys. Rev. B* **88**, 140501 (2013).
26. Y. Nozaki, K. Nakano, T. Yajima, H. Kageyama, B. Frandsen, L. Liu, S. Cheung, T. Goko, Y. J. Uemura, T. S. J. Munsie, T. Medina, G. M. Luke, J. Munevar, D. Nishio-Hamane, C. M. Brown,

Muon spin relaxation and electron/neutron diffraction studies of $BaTi_2(As_{1-x}Sb_x)_2O$: Absence of static magnetism and superlattice reflections. *Phys. Rev. B* **88**, 214506 (2013).
27. Y. Yu, S. A. Kivelson, Fragile superconductivity in the presence of weakly disordered charge density waves. *Phys. Rev. B* **99**, 144513 (2019).
28. Q.-Y. Wang, Z. Li, W.-H. Zhang, Z.-C. Zhang, J.-S. Zhang, W. Li, H. Ding, Y.-B. Ou, P. Deng, K. Chang, J. Wen, C.-L. Song, K. He, J.-F. Jia, S.-H. Ji, Y.-Y. Wang, L.-L. Wang, X. Chen, X.-C. Ma, Q.-K. Xue, Interface-induced high-temperature superconductivity in single unit-cell fese films on $SrTiO_3$. *Chinese Phys. Lett.* **29**, 037402 (2012).
29. Y. Cao, V. Fatemi, S. Fang, K. Watanabe, T. Taniguchi, E. Kaxiras, P. Jarillo-Herrero, Unconventional superconductivity in magic-angle graphene superlattices. *Nature* **556**, 43–50 (2018).
30. Z. Guguchia, F. von Rohr, Z. Shermadini, A. T. Lee, S. Banerjee, A. R. Wieteska, C. A. Marianetti, B. A. Frandsen, H. Luetkens, Z. Gong, S. C. Cheung, C. Baines, A. Shengelaya, G. Taniashvili, A. N. Pasupathy, E. Morenzoni, S. J. L. Billinge, A. Amato, R. J. Cava, R. Khasanov, Y. J. Uemura, Signatures of the topological s^{+-} superconducting order parameter in the type-II Weyl semimetal T_d-$MoTe_2$. *Nat. Commun.* **8**, 1082 (2017).
31. Y. J. Uemura, G. M. Luke, B. J. Sternlieb, J. H. Brewer, J. F. Carolan, W. N. Hardy, R. Kadono, J. R. Kempton, R. F. Kiefl, S. R. Kreitzman, P. Mulhern, T. M. Riseman, D. L. Williams, B. X. Yang, S. Uchida, H. Takagi, J. Gopalakrishnan, A. W. Sleight, M. A. Subramanian, C. L. Chien, M. Z. Cieplak, G. Xiao, V. Y. Lee, B. W. Statt, C. E. Stronach, W. J. Kossler, X. H. Yu, Universal correlations between T_c and $\frac{n_s}{m^*}$ (carrier density over effective mass) in high-T_c cuprate superconductors. *Phys. Rev. Lett.* **62**, 2317 (1989).
32. H. Luetkens, H.-H. Klauss, M. Kraken, F. J. Litterst, T. Dellmann, R. Klingeler, C. Hess, R. Khasanov, A. Amato, C. Baines, M. Kosmala, O. J. Schumann, M. Braden, J. Hamann-Borrero, N. Leps, A. Kondrat, G. Behr, J. Werner, B. Büchner, The electronic phase diagram of the LaO1−xFxFeAs superconductor. *Nat. Mater.* **8**, 305–309 (2009).
33. J. P. Carlo, Y. J. Uemura, T. Goko, G. J. MacDougall, J. A. Rodriguez, W. Yu, G. M. Luke, P. Dai, N. Shannon, S. Miyasaka, S. Suzuki, S. Tajima, G. F. Chen, W. Z. Hu, J. L. Luo, N. L. Wang, Static magnetic order and superfluid density of RFeAs(O,F) (R=La, Nd, Ce) and LaFePO studied by muon spin relaxation: Unusual similarities with the behavior of cuprate superconductors. *Phys. Rev. Lett.* **102**, 087001 (2009).
34. R. Khasanov, H. Luetkens, A. Amato, H.-H. Klauss, Z.-A. Ren, J. Yang, W. Lu, Z.-X. Zhao, Muon spin rotation studies of $SmFeAsO_{0.85}$ and $NdFeAsO_{0.85}$ superconductors. *Phys. Rev. B* **78**, 092506 (2008).
35. Y. J. Uemura, A. Keren, L. P. Le, G. M. Luke, B. J. Sternlieb, W. D. Wu, J. H. Brewer, R. L. Whetten, S. M. Huang, S. Lin, R. B. Kaner, F. Diederich, S. Donovan, G. Grüner, K. Holczer, Magnetic-field penetration depth in K_3C_{60} measured by muon spin relaxation. *Nature* **352**, 605–607 (1991).
36. V. J. Emery, S. A. Kivelson, Importance of phase fluctuations in superconductors with small superfluid density. *Nature* **374**, 434–437 (1995).
37. E. H. Brandt, Flux distribution and penetration depth measured by muon spin rotation in high-T_c superconductors. *Phys. Rev. B* **37**, 2349–2352 (1988).
38. Z. Guguchia, Z. Shermadini, A. Amato, A. Maisuradze, A. Shengelaya, Z. Bukowski, H. Luetkens, R. Khasanov, J. Karpinski, H. Keller, Muon-spin rotation measurements of the magnetic penetration depth in the iron-based superconductor $Ba_{1-x}Rb_xFe_2As_2$. *Phys. Rev. B* **84**, 094513 (2011).
39. A. Suter, B. M. Wojek, The fitting of the *T*-dependence of the penetration depth with α model was performed using the additional library BMW developped by B.M. Wojek. *Phys. Procedia* **30**, 69–73 (2012).
40. M. Tinkham, *Introduction to Superconductivity* (Krieger Publishing Company, 1975).
41. A. Carrington, F. Manzano, Magnetic penetration depth of MgB2. *Physica C* **385**, 205–214 (2003).
42. H. Padamsee, J. E. Neighbor, C. A. Shiffman, Quasiparticle phenomenology for thermodynamics of strong-coupling superconductors. *J. Low. Temp. Phys.* **12**, 387 (1973).
43. Y. Noat, J. A. Silva-Guillén, T. Cren, V. Cherkez, C. Brun, S. Pons, F. Debontridder, D. Roditchev, W. Sacks, L. Cario, P. Ordejón, A. García, E. Canadell, Quasiparticle spectra of *2H*–$NbSe_2$: Two-band superconductivity and the role of tunneling selectivity. *Phys. Rev. B* **92**, 134510–134518 (2015).
44. T. Yokoya, T. Kiss, A. Chainani, S. Shin, M. Nohara, H. Tagaki, Fermi surface sheet-dependent superconductivity in *2H*–$NbSe_2$. *Science* **294**, 2518–2520 (2001).
45. T. Dvir, F. Massee, L. Attias, M. Khodas, M. Aprili, C. H. L. Quay, H. Steinberg, Spectroscopy of bulk and few-layer superconducting $NbSe_2$ with van der Waals tunnel junctions. *Nat. Commun.* **9**, 598 (2018).
46. S. V. Borisenko, A. A. Kordyuk, V. B. Zabolotnyy, D. S. Inosov, D. Evtushinsky, B. Büchner, A. N. Yaresko, A. Varykhalov, R. Follath, W. Eberhardt, L. Patthey, H. Berger, Two energy gaps and fermi-surface "Arcs" in $NbSe_2$. *Phys. Rev. Lett.* **102**, 166402 (2009).
47. L. P. Le, G. M. Luke, B. J. Sternlieb, W. D. Wu, Y. J. Uemura, J. W. Brill, H. Drulis, Magnetic penetration depth in layered compound $NbSe_2$ measured by muon spin relaxation. *Physic. C* **185**, 2715 (1991).
48. F. Soto, H. Berger, L. Cabo, C. Carballeira, J. Mosqueira, D. Pavuna, P. Toimil, F. Vidal, Electric andmagnetic characterization of $NbSe_2$ single crystals: Anisotropic superconducting fluctuations above T_C. *Physic. C Supercond.* **460**, 789 (2007).
49. B. A. Frandsen, S. C. Cheung, T. Goko, L. Liu, T. Medina, T. S. J. Munsie, G. M. Luke, P. J. Baker, M. P. Jimenez S, G. Eguchi, S. Yonezawa, Y. Maeno, Y. J. Uemura, Superconducting properties of noncentrosymmetric superconductor $CaIrSi_3$ investigated by muon spin relaxation and rotation. *Phys. Rev. B* **91**, 014511 (2015).
50. T. Straub, T. Finteis, R. Claessen, P. Steiner, S. Hüfner, P. Blaha, C. S. Oglesby, E. Bucher, Charge-density-wave mechanism in *2H*-$NbSe_2$: Photoemission results. *Phys. Rev. Lett.* **82**, 4504–4507 (1999).
51. K. Rossnagel, O. Seifarth, L. Kipp, M. Skibowski, D. Voß, P. Krüger, A. Mazur, J. Pollmann, Fermi surface of *2H*-$NbSe_2$ and its implications on the charge density-wave mechanism. *Phys. Rev. Lett.* **64**, 235119 (2001).
52. M. D. Johannes, I. I. Mazin, C. A. Howells, Fermi-surface nesting and the origin of the charge-density wave in $NbSe_2$. *Phys. Rev. B* **73**, 205102 (2006).
53. Y. J. Uemura, L. P. Le, G. M. Luke, B. J. Sternlieb, W. D. Wu, J. H. Brewer, T. M. Riseman, C. L. Seaman, M. B. Maple, M. Ishikawa, D. G. Hinks, J. D. Jorgensen, G. Saito, H. Yamochi, Basic similarities among cuprate, bismuthate, organic, Chevrel-phase, and heavy-fermion superconductors shown by penetration-depth measurements. *Phys. Rev. Lett.* **66**, 2665–2668 (1991).
54. Y. J. Uemura, Condensation, excitation, pairing, and superfluid density in high-T_c superconductors: The magnetic resonance mode as a roton analogue and a possible spin-mediated pairing. *J. Phys. Condens. Matter* **16**, S4515–S4540 (2004).
55. Y. J. Uemura, Energy-scale phenomenology and pairing via resonant spin–charge motion in FeAs, CuO, heavy-fermion and other exotic superconductors. *Physica B* **404**, 3195–3201 (2009).
56. Y. J. Uemura, Commonalities in phase and mode. *Nat. Mater.* **8**, 253–255 (2009).
57. A. Shengelaya, R. Khasanov, D. G. Eshchenko, D. Di Castro, I. M. Savić, M. S. Park, K. H. Him, S.-I. Lee, K. A. Müller, H. Keller, Muon-spin-rotation measurements of the penetration depth of the infinite-layer electron-doped $Sr_{0.9}La_{0.1}CuO_2$ cuprate superconductor. *Phys. Rev. Lett.* **94**, 127001 (2005).
58. H. N. S. Lee, M. Garcia, H. Mckinzie, A. Wold, The low-temperature electrical and magnetic properties of $TaSe_2$ and $NbSe_2$. *J. Solid State Chem.* **1**, 190–194 (1970).
59. R. Bel, K. Behnia, H. Berger, Ambipolar nernst effect in $NbSe_2$. *Phys. Rev. Lett.* **91**, 066602 (2003).
60. V. Vescoli, L. Degiorgi, H. Berger, L. Forró, Dynamics of correlated two-dimensional materials: The 2H-$TaSe_2$ case. *Phys. Rev. Lett.* **81**, 453 (1998).
61. D. LeBoeuf, N. Doiron-Leyraud, J. Levallois, R. Daou, J.-B. Bonnemaison, N. E. Hussey, L. Balicas, B. J. Ramshaw, R. Liang, D. A. Bonn, W. N. Hardy, S. Adachi, C. Proust, L. Taillefer, Electron pockets in the Fermi surface of hole-doped high-T_c superconductors. *Nature* **450**, 533–536 (2007).
62. T. Valla, A. V. Fedorov, P. D. Johnson, P.-A. Glans, C. McGuinness, K. E. Smith, E. Y. Andrei, H. Berger, Quasiparticle spectra, charge-densitywaves, superconductivity, and electron-phonon coupling in 2H-$NbSe_2$. *Phys. Rev. Lett.* **92**, 086401 (2004).
63. S. V. Borisenko, A. A. Kordyuk, A. N. Yaresko, V. B. Zabolotnyy, D. S. Inosov, R. Schuster, B. Büchner, R. Weber, R. Follath, L. Patthey, H. Berger, Pseudogap and charge density waves in two dimensions. *Phys. Rev. Lett.* **100**, 196402 (2008).
64. A. A. Kordyuk, S. V. Borisenko, V. B. Zabolotnyy, R. Schuster, D. S. Inosov, D. V. Evtushinsky, A. I. Plyushchay, R. Follath, A. Varykhalov, L. Patthey, H. Berger, Nonmonotonic pseudogap in high-T_c cuprates. *Phys. Rev. B* **79**, 020504 (2009).
65. S. V. Borisenko, A. A. Kordyuk, V. B. Zabolotnyy, D. S. Inosov, D. Evtushinsky, B. Büchner, A. N. Yaresko, A. Varykhalov, R. Follath, W. Eberhardt, L. Patthey, H. Berger, Two energy gaps and fermi-surface "Arcs" in $NbSe_2$. *Phys. Rev. Lett.* **102**, 166402 (2009).
66. T. Hanaguri, C. Lupien, Y. Kohsaka, D.-H. Lee, M. Azuma, M. Takano, H. Takagi, J. C. Davis, A 'checkerboard' electronic crystal state in lightly hole-doped $Ca_{2-x}Na_xCuO_2Cl_2$. *Nature* **430**, 1001 (2004).
67. Y. Kohsaka, C. Taylor, K. Fujita, A. Schmidt, C. Lupien, T. Hanaguri, M. Azuma, M. Takano, H. Eisaki, H. Takagi, S. Uchida, J. C. Davis, An intrinsic bond-centered electronic glass with unidirectional domains in underdoped cuprates. *Science* **315**, 1380–1385 (2007).
68. R. Khasanov, Z. Guguchia, A. Maisuradze, D. Andreica, M. Elender, A. Raselli, Z. Shermadini, T. Goko, F. Knecht, E. Morenzoni, A. Amato, High pressure research using muons at the Paul Scherrer Institute. *High Press. Res.* **36**, 140–166 (2016).
69. D. Andreica, thesis, IPP/ETH-Zürich (2001).
70. A. Maisuradze, A. Shengelaya, A. Amato, E. Pomjakushina, H. Keller, Muon spin rotation investigation of the pressure effect on the magnetic penetration depth in $YBa_2Cu_3O_x$. *Phys. Rev. B* **84**, 184523 (2011).
71. Z. Guguchia, A. Amato, J. Kang, H. Luetkens, P. K. Biswas, G. Prando, F. von Rohr, Z. Bukowski, A. Shengelaya, H. Keller, E. Morenzoni, R. M. Fernandes, R. Khasanov, Direct evidence for the emergence of a pressure induced nodal superconducting gap in the iron-based superconductor $Ba_{0.65}Rb_{0.35}Fe_2As_2$. *Nat. Commun.* **6**, 8863 (2015).

72. J. E. Sonier, J. H. Brewer, R. F. Kiefl, μSR studies of the vortex state in type-II superconductors. *Rev. Mod. Phys.* **72**, 769–811 (2000).
73. Z. Guguchia, R. Khasanov, A. Shengelaya, E. Pomjakushina, S. J. L. Billinge, A. Amato, E. Morenzoni, H. Keller, Cooperative coupling of static magnetism and bulk superconductivity in the stripe phase of $La_{2-x}Ba_xCuO_4$: Pressure- and doping-dependent studies. *Phys. Rev. B* **94**, 214511 (2016).

Acknowledgments: The μSR experiments were carried out at the Swiss Muon Source (SμS) Paul Scherrer Insitute, Villigen, Switzerland. **Funding:** Z.G. acknowledges the financial support by the Swiss National Science Foundation (SNF fellowship P300P2-177832). The work at the University of Zurich was supported by the Swiss National Science Foundation under grant no. PZ00P2_174015. Work at Department of Physics of Columbia University was supported by U.S. NSF DMR-1436095 (DMREF) and NSF DMR-1610633. M.Z.H. was supported by U.S. DOE/BES grant no. DE-FG-02-05ER46200. R.K. acknowledges the Swiss National Science Foundation (grants 200021_149486 and 200021_175935). A.N. acknowledges funding from the European Union's Horizon 2020 Research and Innovation Programme under the Marie Sklodowska-Curie grant agreement no. 701647. **Author contributions:** Project planning: Z.G. and F.O.v.R. Sample growth: F.O.v.R. and C.W. Experiments and corresponding discussions: Z.G., J.-C.O., R.K., Z.S., A.N., A.R.W., A.N.P., J.C., M.Z.H., A.A., H.L., and Y.J.U. μSR data analysis: Z.G. Data interpretation and draft writing: Z.G. and F.O.v.R. with contributions and/or comments from all authors. **Competing interests:** The authors declare that they have no competing interests. **Data and materials availability:** All data needed to evaluate the conclusions in the paper are present in the paper. Additional data related to this paper may be requested from the authors.

Submitted 6 November 2018
Accepted 17 September 2019
Published 29 November 2019
10.1126/sciadv.aav8465

Citation: F. O. von Rohr, J.-C. Orain, R. Khasanov, C. Witteveen, Z. Shermadini, A. Nikitin, J. Chang, A. R. Wieteska, A. N. Pasupathy, M. Z. Hasan, A. Amato, H. Luetkens, Y. J. Uemura, Z. Guguchia, Unconventional scaling of the superfluid density with the critical temperature in transition metal dichalcogenides. *Sci. Adv.* **5**, eaav8465 (2019).